results indicate that the picture becomes blurry in the domain of long, weak bonds as encountered in f-metal complexes. The orientation of the hmb ligand, obviously not an anionic ligand, is clearly determined by steric interactions. Moreover, reducing the size of the central atom entails a rearrangement which affects the entire coordination sphere. The resulting differences in the lengths of equivalent bonds span a range comparable to the difference in ionic radii, the π-bonds of the neutral arene and the σ-bonds of the ionic $AlCl_4$ ligands being affected equally. We therefore conclude that the small structural changes in complexes with weakly bonded ligands are not suitable criteria for the evaluation of the nature of the bonds.

Acknowledgment. This work was supported by The Robert A. Welch Foundation (Grant No. A-494).

Supplementary Material Available: A full list of bond distances and angles and tables of anisotropic thermal parameters (9 pages); listings of observed and calculated structure factors (26 pages). Ordering information is given on current masthead page.

Metal Alkoxides—Models for Metal Oxides. 12.[1] The First Molecular Carbido Cluster of Tungsten $W_4(C)(NMe)(O\text{-}i\text{-}Pr)_{12}$ and ^{13}C NMR Spectroscopic Evidence for a Related Oxo–Carbido Cluster, $W_4(C)(O)(O\text{-}i\text{-}Pr)_{12}$, Formed in the Stepwise Reductive Cleavage of Carbon Monoxide by Lower Valent Tungsten Alkoxides

Malcolm H. Chisholm,* David L. Clark, John C. Huffman, and Crystal A. Smith

Department of Chemistry and Molecular Structure Center, Indiana University, Bloomington, Indiana 47405

Received November 17, 1986

The first molecular carbido tungsten cluster compound $W_4(C)(NMe)(O\text{-}i\text{-}Pr)_{12}$ is formed as a minor component in the reaction between $W_2(NMe_2)_6$ and *i*-PrOH (≫6 equiv). The black crystalline compound has been characterized by elemental analysis, mass spectroscopy, ^1H and ^{13}C NMR spectroscopy, cyclic voltammetry, and a single-crystal X-ray study. There is a butterfly of tungsten atoms with five W–W edge distances of ca. 2.80 Å supported by bridging O-*i*-Pr ligands. The unique NMe ligand bridges a backbone–wingtip edge such that the molecule has no virtual element of symmetry. The $W_4(\mu\text{-}C)$ distances fall into two categories: backbone–W–C = 2.25 Å and wingtip–W–C = 1.93 Å (av). The bonding in this carbido cluster has been investigated by calculations employing the Fenske–Hall method on the $W_4(C)(OH)_{13}^+$ model cation constrained to C_{2v} symmetry. The results of this calculation are compared with those recently reported for "iron-butterfly" carbido clusters, $Fe_4(\mu_4\text{-}C)$, supported by carbonyl ligands. The high-valent early-transition-metal and low-valent later transition-metal $M_4(\mu_4\text{-}C)$ clusters are related by an isolobal d^3–d^9 "hole formalism". In both the $W_4(\mu_4\text{-}C)$ and $Fe_4(\mu_4\text{-}C)$ clusters the stronger carbon-to-metal bonding to the wingtip metal atoms is reflected by (i) the shorter M–C distances and (ii) the atomic overlap population between the metal and carbon orbitals. The tungsten cluster shows a significant bonding interaction with the C 2s atomic orbital; this situation is not found in the $Fe_4(\mu_4\text{-}C)$ clusters. Spectroscopic evidence, based solely on ^{13}C NMR data, is presented for the formation of an isoelectronic and isostructural carbido–oxide cluster, $W_4(C)(O)(O\text{-}i\text{-}Pr)_{12}$, in the reaction between carbon monoxide and $W_2(O\text{-}t\text{-}Bu)_6$ (2 equiv) followed by addition of *i*-PrOH (≫12 equiv). The stepwise sequence of C—O and W—W bond order reduction provides an extension to earlier studies of the reaction W≡W + C≡O → (W═W)(μ-C═O) → [(W-W)(μ-C-O)]$_2$: *Organometallics* **1986**, *5*, 2125. Crystal data for $W_4(C)(NMe)(O\text{-}i\text{-}Pr)_{12}$ at −165 °C: a = 19.379 (1) Å, b = 12.516 (1) Å, c = 11.883 (1) Å, α = 119.37 (6)°, β = 84.98 (5)°, γ = 98.79 (5)°, Z = 2, d_{calcd} = 1.988 g cm^{-3}, and space group $P\bar{1}$.

Introduction

Central to the theme of this research is the compatibility of ligands such as hydride, alkyl, aryl, alkylidene, alkylidyne, carbide (C_2 or C_1), etc. with cluster fragments of molybdenum and tungsten supported exclusively by alkoxide and/or oxide/alkoxide ligands. We have suggested that compounds formed from these ligands and the cluster fragments may provide models for the organometallic chemistry which occurs on the surfaces of the reduced oxides of these elements.[2] Irrespective of the validity of this suggestion, the organometallic chemistry of alkoxide-supported clusters is of fundamental interest and represents a totally new area of organometallic cluster chemistry. For these compounds to act as models for the reduced oxides, the ratio of alkoxide ligands (representing oxo ligands, either terminal or bridging) to hydrocarbyl ligands (or other ligands of interest, e.g. H or N) must be relatively large. Furthermore, the "organometallic" ligand to metal ratio should be small, in general less than one, although cluster compounds in which one metal atom is

(1) Part 11: Chisholm, M. H.; Eichhorn, B. W.; Folting, K.; Huffman, J. C.; Tatz, R. J. *Organometallics* **1986**, *5*, 1599.

(2) (a) Chisholm, M. H. *ACS Symp. Ser.* **1983**, *No. 211*, 243. (b) Chisholm, M. H. *J. Solid State Chem.* **1985**, *57*, 120.

0276-7333/87/2306-1280$01.50/0

bonded to two or more functionalities are also of interest. Within these criteria the chemistry of compounds such as $W_3(\mu_3\text{-CR})(OR')_9$,[3] $W_4(\mu\text{-H})_2(O\text{-}i\text{-Pr})_{14}$,[4] $W_3(\mu_3\text{-NH})(O\text{-}i\text{-Pr})_{10}$,[5] and $Mo_4(\mu_3\text{-N})_2(O\text{-}i\text{-Pr})_{12}$[6] is thus of particular interest.

We describe here our isolation and characterization of the first carbido tungsten cluster compound $W_4(C)(NMe)(O\text{-}i\text{-Pr})_{12}$ in which the carbido ligand is supported by a butterfly of tungsten atoms.[7] We present spectroscopic evidence for the formation of an isoelectronic (and isostructural) oxo compound, $W_4(C)(O)(O\text{-}i\text{-Pr})_{12}$, by a stepwise reductive cleavage of C≡O in its reactions with lower valent tungsten alkoxides. A comparison of the bonding in the W_4–carbido compound with that previously described for $Fe_4(C)(CO)_{12}^{2-}$ is forwarded on the basis of MO calculations employing the Fenske–Hall method on the model compound $W_4(C)(OH)_{13}^{+}$.

Results and Discussion

Synthesis of $W_4(C)(NMe)(O\text{-}i\text{-Pr})_{12}$. Samples of $W_2(O\text{-}i\text{-Pr})_6(HNMe_2)_2$[8] formed in the reaction shown in eq 1 are always contaminated with small quantities of a black crystalline compound, $W_4(C)(NMe)(O\text{-}i\text{-Pr})_{12}$.

$$W_2(NMe_2)_6 + i\text{-PrOH(excess)} \xrightarrow[\text{hexane}/i\text{-PrOH}]{0\ ^\circ\text{C, 1 h}} W_2(O\text{-}i\text{-Pr})_6(HNMe_2)_2 + 4HNMe_2 \quad (1)$$

Upon recrystallization from hexane $W_2(O\text{-}i\text{-Pr})_6(HNMe_2)_2$ forms large cubic crystals that are easily hand-separated from the bulk microcrystalline sample. Thus recrystallizations from hexane followed by removal of the large crystals of $W_2(O\text{-}i\text{-Pr})_6(HNMe_2)_2$ leaves a crude mixture enriched in $W_4(C)(NMe)(O\text{-}i\text{-Pr})_{12}$. Recrystallization of the residue from three such separations employing a CH_2Cl_2/i-PrOH solvent mixture yields $W_4(C)(NMe)(O\text{-}i\text{-Pr})_{12}$ as a black crystalline compound. From this rather tedious process we have isolated in total ca. 500 mg of analytically pure $W_4(C)(NMe)(O\text{-}i\text{-Pr})_{12}$ during the course of these studies. Clearly this is not a very satisfactory synthesis, but we are confident we shall be able to find alternate syntheses of $W_4(\mu\text{-C})$-containing compounds.

Though not central to the theme of this paper, one might want to speculate, or at least comment, on how $W_4(C)(NMe)(O\text{-}i\text{-Pr})_{12}$ could be formed in reaction 1. First it should be stated that it is *not* formed by the thermal decomposition of $W_2(O\text{-}i\text{-Pr})_6(HNMe_2)_2$. Loss of $HNMe_2$ gives $W_4(O\text{-}i\text{-Pr})_{12}$ while in the presence of $HNMe_2$ and i-PrOH a further reaction leads to $W_4(H)_2(O\text{-}i\text{-Pr})_{14}$.[8] We conclude that $W_4(C)(NMe)(O\text{-}i\text{-Pr})_{12}$ is formed during the alcoholysis reaction; i.e., its formation is competitive with that of $W_2(O\text{-}i\text{-Pr})_6(HNMe_2)_2$. The isolated yield of $W_2(O\text{-}i\text{-Pr})_6(HNMe_2)_2$ according to the stoichiometry shown in eq 1 is ca. 80%, and the yield of $W_4(C)(NMe)(O\text{-}i\text{-Pr})_{12}$ is typically in the range 5–10%. The ability of the $(W{\equiv}W)^{6+}$ unit to activate NMe_2 ligands was recently seen in a hydrogen atom transfer reaction leading to the formation of a $W_2(\mu\text{-}CH_2NMe)$ moiety for which structural and spectroscopic data were consistent with a CH_2–N single bond.[9] Such a species may well be involved in the initial stages of the conversion of a NMe_2 ligand to NMe and C groups.

Characterization of $W_4(C)(NMe)(O\text{-}i\text{-Pr})_{12}$. The characterization of this compound rests on a number of the spectroscopic techniques together with a single-crystal X-ray crystallographic determination and can be briefly summarized as follows. Elemental analysis clearly identifies the presence of nitrogen and in the predicted amount. The ^1H NMR spectrum (at 360 MHz) shows the presence of several different O-i-Pr ligands, and indeed 12 methyne septets can be identified for the 12 inequivalent O-i-Pr ligands. Though some of the C*H* resonances are overlapping the molecule is not fluxional below +60 °C in toluene-d_8. A singlet at ca. δ 5 ppm is assignable to the N*Me* group, and in the ^{13}C spectrum a signal assignable to this moeity is identified by the appearance of a 1:3:3:1 quartet in the proton coupled spectrum. The molecule shows a very weak M^+ ion in the mass spectrum. The isotope distribution and mass determination under low resolution clearly identify this as $W_4(C)(NMe)(O\text{-}i\text{-Pr})_{12}^{+}$. In the ^{13}C NMR spectrum in toluene-d_8, employing $Cr(acac)_3$ as a shiftless relaxation agent, a signal at δ 367 is assignable to the μ_4-C atom.[10] In the ^1H-coupled spectrum this signal remains a singlet indicative of its quaternary nature and consistent with the absence of any two-bond ^{13}C–^1H couplings. No satellite spectrum from coupling to the ^{183}W nuclei, $I = {}^1/_2$, 14.5% natural abundance was resolvable, however, because of the poor signal to noise of this resonance using natural abundance ^{13}C samples. The crystallography readily identified the μ_2-NMe ligand: the W–N distances are, for example, unacceptable for a μ-OMe ligand. Also the μ_4-C atom and the μ_2-N atom of the NMe ligand were refined as fractions of C/N/O with the result that the NMe nitrogen converged to 5% O and 95% N while the carbido carbon converged to 85% C and 15% O. No hydride ligands were detectable by ^1H NMR spectroscopy nor were any implicated by holes or trans influences in the molecular structure. We conclude that the compound is accurately formulated as $W_4(C)(NMe)(O\text{-}i\text{-Pr})_{12}$.

Molecular Structure of $W_4(C)(NMe)(O\text{-}i\text{-Pr})_{12}$. Stereoviews of the molecule are given in Figure 1, and a ball-and-stick drawing of the central W_4CNO_{12} moiety is given in Figure 2. Figures showing the full atom numbering scheme are given in the supplementary materials. Fractional coordinates are given in Table I, and a summary of crystal data is given in Table II. Selected bond distances and bond angles are given in Tables III and IV, respectively.

The four tungsten atoms form a butterfly or opened tetrahedron with W–W bonding distances of 2.80 (1) Å with the exception of the W(2)–W(4) distance which is significantly shorter, 2.747 (2) Å, and is the unique edge being bridged by the NMe ligand. If charge is partitioned to the ligands as C^{4-}, NMe^{2-}, and O-i-Pr^-, the W_4 unit carries a formal charge of +18 and there are thus six electrons available for M–M bonding. This is worthy of mention only because the five W–W distances of ca. 2.8 Å are so much longer than the Mo–Mo distances in the 12-electron Mo_4 butterfly clusters $Mo_4Br_4(O\text{-}i\text{-Pr})_8$ and

(3) Chisholm, M. H.; Folting, K.; Heppert, J. A.; Hoffman, D. M.; Huffman, J. C. *J. Am. Chem. Soc.* **1985**, *107*, 1234.
(4) Akiyama, M.; Chisholm, M. H.; Cotton, F. A.; Extine, M. W.; Haitko, D. A.; Leonelli, J.; Little, D. *J. Am. Chem. Soc.* **1981**, *103*, 779.
(5) Chisholm, M. H.; Hoffman, D. M.; Huffman, J. C. *Inorg. Chem.* **1985**, *24*, 796.
(6) Chisholm, M. H.; Folting, K.; Huffman, J. C.; Leonelli, J.; Marchant, N. S.; Smith, C. A.; Taylor, L. C. E. *J. Am. Chem. Soc.* **1985**, *107*, 3722.
(7) A preliminary report noting the discovery of $W_4(C)(NMe)(O\text{-}i\text{-Pr})_{12}$ and $Mo_4(N)_2(O\text{-}i\text{-Pr})_{12}$ has appeared: ref 6.
(8) Chisholm, M. H.; Huffman, J. C.; Smith, C. A. *J. Am. Chem. Soc.* **1986**, *108*, 222.
(9) Ahmed, K. J.; Chisholm, M. H.; Folting, K.; Huffman, J. C. *J. Am. Chem. Soc.* **1980**, *108*, 989.
(10) This is well within the range seen for other carbido carbon atoms in $M_4(\mu\text{-C})$-containing species. For general reviews of carbido metal clusters see: Bradley, J. S. *Adv. Organomet. Chem.* **1983**, 22. Tachikawa, M.; Muetterties, E. L. *Prog. Inorg. Chem.* **1981**, *28*, 203.

Table I. Fractional Coordinates and Isotropic Thermal Parameters for the $W_4(C)(NMe)(O\text{-}i\text{-}Pr)_{12}$ Molecule

atom	10^4x	10^4y	10^4z	$10B_{iso}$, Å^2
W(1)	3077.2 (3)	5866 (1)	7012 (1)	13
W(2)	1659.1 (3)	6969 (1)	9647 (1)	12
W(3)	3122.2 (3)	7090 (1)	9712 (1)	11
W(4)	2274.3 (3)	4832 (1)	8414 (1)	11
O(5)	2647 (5)	5001 (10)	5417 (10)	19
C(6)	2020 (8)	4524 (16)	4680 (15)	23
C(7)	2167 (11)	3314 (18)	3477 (18)	40
C(8)	1809 (8)	5436 (17)	4354 (18)	29
O(9)	3507 (5)	7102 (9)	6575 (9)	15
C(10)	3477 (8)	7263 (15)	5485 (14)	21
C(11)	4212 (9)	7516 (19)	5047 (16)	32
C(12)	3064 (10)	8323 (18)	5805 (20)	38
O(13)	1266 (5)	8452 (10)	10931 (10)	20
C(14)	625 (8)	5934 (14)	11034 (16)	19
C(15)	201 (8)	8933 (16)	12137 (17)	26
C(16)	804 (8)	10250 (16)	11211 (17)	23
O(17)	866 (5)	6747 (9)	8651 (10)	18
C(18)	788 (8)	6679 (19)	7450 (15)	28
C(19)	2 (9)	6390 (16)	7199 (19)	31
C(20)	1080 (8)	7838 (18)	7477 (18)	28
O(21)	3341 (5)	8711 (9)	9913 (10)	28
C(22)	3065 (8)	9456 (16)	9502 (14)	29
C(23)	2681 (9)	10380 (15)	10632 (19)	27
C(24)	3647 (9)	10094 (15)	9055 (18)	28
O(25)	3840 (5)	7622 (9)	11068 (9)	14
C(26)	4364 (7)	8641 (14)	11580 (16)	17
C(27)	4959 (7)	8282 (15)	11998 (16)	20
C(28)	4102 (9)	9764 (17)	12662 (18)	33
O(29)	1678 (5)	3973 (9)	6904 (10)	14
C(30)	1093 (7)	3031 (14)	6695 (15)	17
C(31)	1239 (9)	1853 (17)	5466 (19)	32
C(32)	447 (7)	3468 (15)	6579 (16)	24
O(33)	2210 (5)	3205 (10)	8472 (11)	25
C(34)	1757 (9)	2553 (16)	8949 (17)	27
C(35)	1903 (9)	2975 (18)	10314 (18)	30
C(36)	1831 (11)	1194 (18)	8089 (21)	40
O(37)	3022 (5)	5454 (9)	9768 (9)	12
C(38)	3376 (8)	4878 (15)	10305 (16)	22
C(39)	3281 (8)	5496 (17)	11740 (15)	20
C(40)	4100 (8)	4804 (17)	9859 (17)	27
O(41)	3863 (5)	6487 (10)	8316 (10)	15
C(42)	4614 (7)	6653 (16)	8308 (15)	20
C(43)	4879 (8)	5499 (17)	7222 (16)	28
C(44)	4896 (8)	7786 (16)	8208 (14)	19
O(45)	3103 (4)	4255 (9)	7033 (9)	9
C(46)	3171 (8)	3018 (15)	5928 (15)	18
C(47)	3419 (9)	2264 (16)	6422 (18)	32
C(48)	3653 (8)	3112 (17)	4919 (18)	29
O(49)	2390 (5)	7657 (9)	11115 (9)	30
C(50)	2358 (8)	8133 (16)	12492 (16)	22
C(51)	1776 (8)	7375 (17)	12808 (16)	25
C(52)	2288 (9)	9483 (17)	13222 (18)	30
C(53)	894 (9)	4959 (17)	10230 (19)	36
N(54)	1482 (6)	5416 (12)	9647 (12)	15
C(55)	2321 (7)	6520 (13)	8193 (14)	13

$Mo_4Br_3(O\text{-}i\text{-}Pr)_9$ that average 2.5 Å.[11]

The W–O bond distances fall in the expected ranges W–O(terminal) = 1.90 (3) Å and W–O(bridging) = 2.03 (3) Å. Note there are no triply bridging alkoxides in this molecule and that the W–N distances associated with the μ-NMe ligand, 1.92 and 1.98 Å, are shorter than those associated with the μ-O-*i*-Pr ligands. It can also be noted that examination of the packing (space-filling model diagrams) around the NMe ligands indicates there is insufficient space for two additional methyl groups as would be required for a μ-O-*i*-Pr ligand.

The carbido carbon atom is strongly bonded to the wingtip tungsten atoms W(1) and W(2) as evidenced by the very short W–C distances, 1.914 (14) and 1.956 (15) Å, respectively, whereas the C to W distances involving the backbone tungsten atoms are much longer, 2.24 (3) Å (averaged). The angles subtended by the carbido carbon to the wingtip and backbone tungsten atoms are 163.5 (8) and 77.0 (4)°, respectively. In these respects the central $W_4(\mu_4\text{-}C)$ moiety resembles other $M_4(\mu_4\text{-}C)$ moieties supported by carbonyl ligands.[10,12]

The backbone tungsten atoms are coordinated to six ligand atoms in a distorted octahedral geometry while the wingtip tungsten atoms are coordinated to only five ligand atoms. The geometry about the latter may be viewed as distorted square-based pyramids. The μ-NMe ligand bridges a backbone and a wingtip tungsten atom which renders the molecule with no virtual element of symmetry. Nevertheless the $W_4(C)(NMe)(O\text{-}i\text{-}Pr)_{12}$ molecule bears at least a superficial resemblance to the well-known "iron-butterfly" $Fe_4(C)(CO)_{13}$.[12]

Table II. Summary of Crystal Data for the $W_4(C)(NMe)(O\text{-}i\text{-}Pr)_{12}$ Molecule

empirical formula	$W_4O_{12}C_{38}NH_{87}$
color of cryst	black
cryst dimens, mm	0.05 × 0.14 × 0.24
space group	$P\bar{1}$
cell dimens	
temp, °C	−165
a, Å	19.379 (0)
b, Å	12.516 (0)
c, Å	11.883 (0)
α, deg	119.37 (6)
β, deg	84.98 (5)
γ, deg	98.79 (5)
Z (molecules/cell)	2
V Å^3	0.00
d(calcd), g/cm^3	1.988
wavelength, Å	0.710 69
mol wt	1485.50
linear abs coeff, cm	94.338
detector to sample dist, cm	22.5
sample to source dist, cm	23.5
av Ω scan width at half-height, deg	0.25
scan speed, deg/min	4.0
scan width (deg + dispersion)	2.0
individual bkgd, s	5
aperture size, mm	3.0 × 4.0
2θ range, deg	6–45
total no. of reflctns collected	7381
no. of unique intensities	5867
no. with $F > 0.0$	5413
no. with $F > \sigma(F)$	5147
no. with $F > 2.3\ \sigma(F)$	4770
$R(F)$	0.0539
$R_w(F)$	0.0462
goodness of fit for the last cycle	1.567
max Δ/σ for last cycle	0.05

Electronic Structure and Bonding in Alkoxide-Supported Tungsten Carbide Clusters. We have employed the Fenske–Hall molecular orbital method[13] to obtain numerical results for comparison with the recent theoretical results for Fe_4C carbido clusters,[14-16] and we will show in a very satisfying way some remarkable similarities and differences between the W_4C and Fe_4C clusters. To make the computation more tractable, the bonding in a model cluster of formula $W_4C(OH)_{13}^+$ was examined in an idealized C_{2v} geometry. If for the sake of electron counting, charge in $W_4C(NMe)(O\text{-}i\text{-}Pr)_{12}$ is partitioned

(11) (a) Chisholm, M. H.; Errington, R. J.; Folting, K.; Huffman, J. C. *J. Am. Chem. Soc.* **1982**, *104*, 2025; (b) Clark, D. L. Ph.D. Thesis, Indiana University, 1986.

(12) Bradley, J. S.; Ansell, J. B.; Leonowicz, M. E.; Hill, E. W. *J. Am. Chem. Soc.* **1981**, *103*, 4968.

(13) Hall, M. B.; Fenske, R. F. *Inorg. Chem.* **1972**, *11*, 768.

(14) Harris, S.; Bradley, J. S. *Organometallics* **1984**, *3*, 1086.

(15) Wijeyesekera, S. D.; Hoffmann, R.; Wilker, C. N. *Organometallics* **1984**, *3*, 962.

(16) Wijeyesekera, S. D.; Hoffmann, R. *Organometallics* **1984**, *3*, 949.

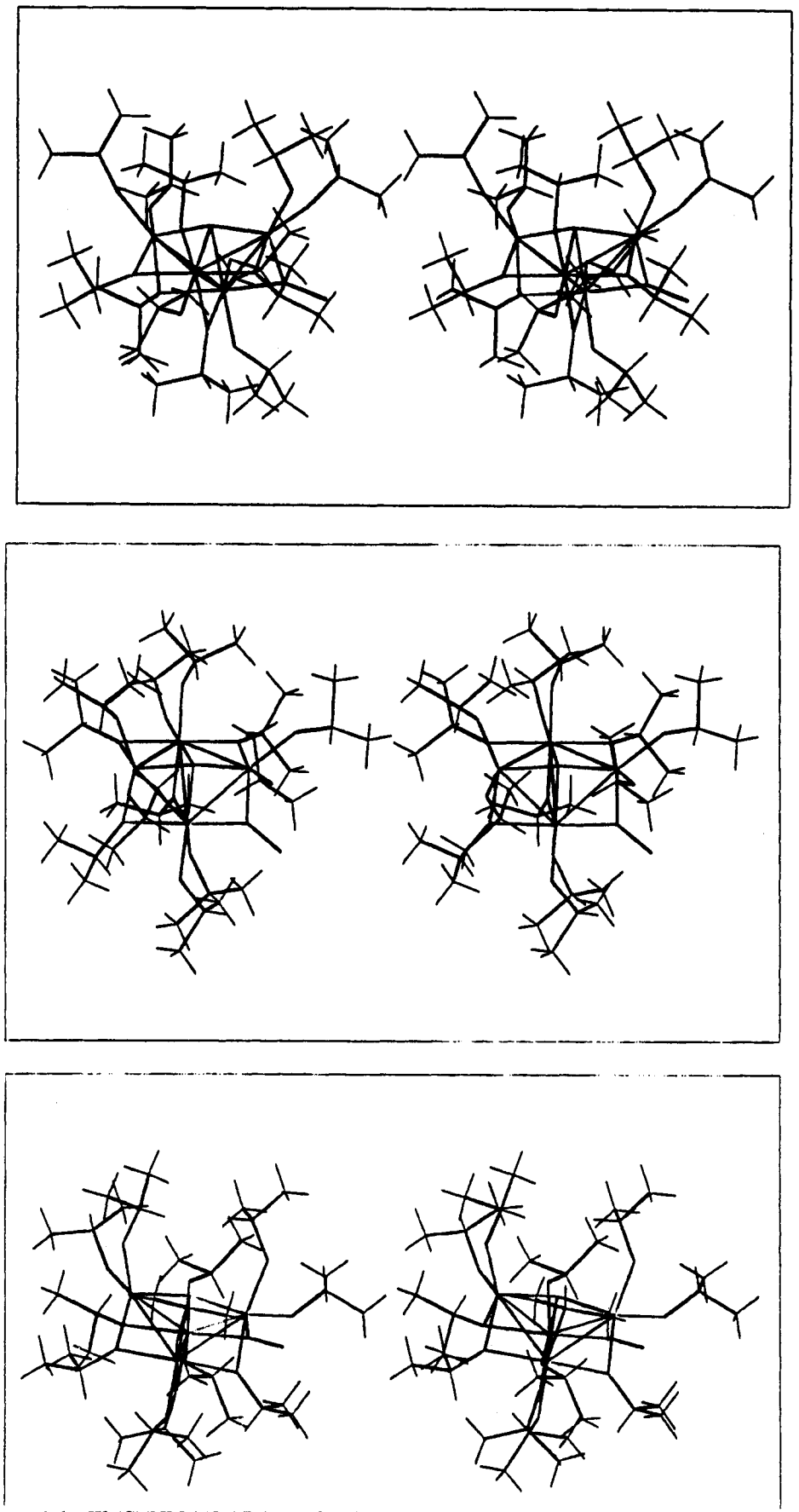

Figure 1. Stereoviews of the $W_4(C)(NMe)(O\text{-}i\text{-}Pr)_{12}$ molecule.

between the metal atoms and the ligands as C^{4-}, NMe^{2-}, and O-*i*-Pr^-, then the tetranuclear center is formally W_4^{18+} having only six electrons for metal–metal cluster bonding, as noted before. This, of course, is a pervasive formalism used in the field, and it will be demonstrated that a mixing of metal–metal and metal–ligand bonding, particularly with carbon, will complicate this simple formalism. Clearly, the five W–W distances, 2.80 Å (averaged), within

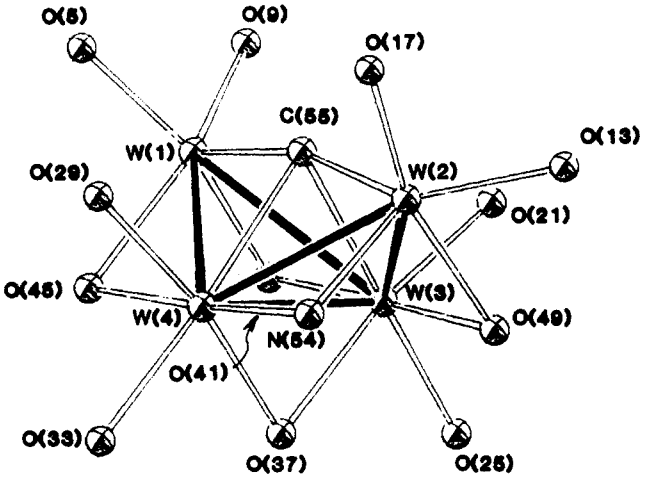

Figure 2. A ball-and-stick drawing of the central W_4CNO_{12} unit of the $W_4(C)(NMe)(O\text{-}i\text{-}Pr)_{12}$ molecule giving the atom number scheme used in the Tables.

Table III. Selected Bond Distances (Å) for the $W_4(C)(NMe)(O\text{-}i\text{-}Pr)_{12}$ Molecule

A	B	dist
W(1)	W(3)	2.799 (2)
W(1)	W(4)	2.814 (2)
W(1)	O(5)	1.857 (10)
W(1)	O(9)	1.917 (10)
W(1)	O(41)	2.048 (10)
W(1)	O(45)	2.037 (10)
W(1)	C(55)	1.914 (14)
W(2)	W(3)	2.822 (1)
W(2)	W(4)	2.747 (2)
W(2)	O(13)	1.950 (11)
W(2)	O(17)	1.925 (9)
W(2)	O(49)	2.093 (12)
W(2)	N(54)	1.922 (13)
W(2)	C(55)	1.956 (15)
W(3)	W(4)	2.795 (3)
W(3)	O(21)	1.907 (12)
W(3)	O(25)	2.008 (9)
W(3)	O(37)	2.060 (10)
W(3)	O(41)	2.018 (9)
W(3)	O(49)	2.007 (11)
W(3)	C(55)	2.251 (14)
W(4)	O(29)	1.951 (10)
W(4)	O(33)	2.056 (12)
W(4)	O(37)	2.031 (10)
W(4)	O(45)	2.127 (9)
W(4)	N(54)	1.984 (12)
W(4)	C(55)	2.241 (14)
O(5)	C(6)	1.431 (18)
O(9)	C(10)	1.412 (19)
O(13)	C(14)	1.432 (17)
O(17)	C(18)	1.408 (19)
O(21)	C(22)	1.427 (23)
O(25)	C(26)	1.406 (18)
O(29)	C(30)	1.445 (17)
O(33)	C(34)	1.381 (21)
O(37)	C(38)	1.442 (19)
O(41)	C(42)	1.438 (17)
O(45)	C(46)	1.475 (18)
O(49)	C(50)	1.439 (20)
N(54)	C(53)	1.469 (21)

the W_4 butterfly core imply a significant W–W interaction.

For purposes of comparison we can envision the formation of $W_4C(OH)_{13}^+$ from the fragments $W_4(OH)_{13}^{3-}$ and C^{4+}. This hypothetical situation allows us to consider first the bonding in the alkoxide-supported tungsten butterfly cluster and then consider the interaction of the butterfly with a carbon atom to form the alkoxide-supported tungsten carbide cluster. The molecular orbital diagram for $W_4(OH)_{13}^{3-}$ is shown on the left of Figure 3. Those

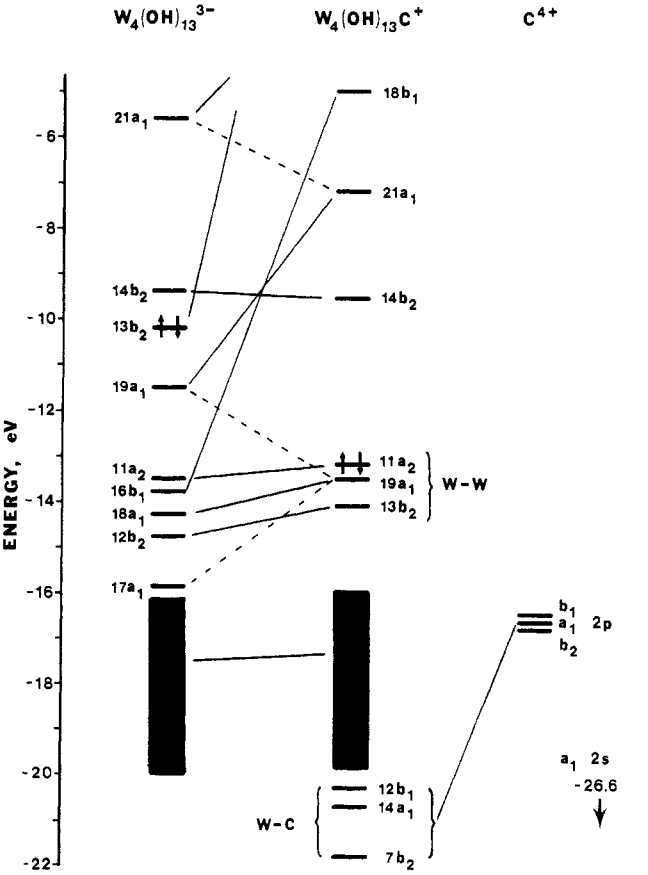

Figure 3. Fragment molecular orbital diagram showing the perturbation of $W_4(OH)_{13}^{3-}$ cluster fragment orbitals by interaction with the carbon atom. The HOMO's in each case are denoted by arrows. Only the important metal–metal and metal–carbon bonding orbitals are shown.

orbitals above and including $17a_1$ are primarily W–W cluster bonding in character. The $W_4(OH)_{13}^{3-}$ cluster can be considered to be constructed from four mononuclear $W(OH)_n$ (n = 4 or 5) octahedral fragments as follows. The local WO_4 geometry about the wingtip atoms is essentially that of a square-based pyramid with the oxygen atoms making up the basal sites with the vacant apical position directed toward the missing carbon atom. In a similar fashion, the local WO_5 geometry about the backbone tungsten atoms is that of an octahedron with one missing vertex; this site is also directed toward the missing carbon atom. In this fashion, we may view the MOs of $W_4(OH)_{13}^{3-}$ as being derived from the interaction of ML_5 (backbone) and ML_4 (wingtip) octahedral fragments. Of particular interest are the $13b_2$, $19a_1$, $16b_1$, and $17a_1$ metal–metal cluster bonding orbitals of $W_4(OH)_{13}^{3-}$ that are directed toward the site of the missing carbon atom and have the proper symmetry to interact with carbon atomic orbitals.

The interaction of $W_4(OH)_{13}^{3-}$ with carbon 2s and 2p atomic orbitals in Figure 3 occurs primarily with four occupied frontier orbitals of symmetry a_1, a_1, b_1, and b_2 under C_{2v} symmetry. The carbon 2s orbital lies very low in energy and is not shown in Figure 3. The principal result of the interaction of the frontier orbitals of $W_4(OH)_{13}^{3-}$ with carbon 2p atomic orbitals is formation of three W–C bonding orbitals, $12b_1$, $14a_1$, and $7b_2$, that are well-separated energetically from the manifold of W–W cluster bonding orbitals. The fact that these orbitals are so much lower in energy than the W–W cluster bonding orbitals reflects the greater strength of metal–carbon bonding than metal–metal bonding in the W_4C cluster. The main interaction involving the carbon 2s orbital is formation of

Table IV. Selected Bond Angles (deg) for the $W_4(C)(NMe)(O\text{-}i\text{-}Pr)_{12}$ Molecule

A	B	C	angle	A	B	C	angle	A	B	C	angle
W(3)	W(1)	W(4)	59.7 (1)	W(1)	W(3)	O(41)	46.9 (3)	W(3)	W(4)	O(37)	47.3 (3)
W(3)	W(1)	O(5)	155.3 (3)	W(1)	W(3)	O(49)	133.7 (3)	W(3)	W(4)	O(45)	86.6 (3)
W(3)	W(1)	O(9)	103.5 (3)	W(1)	W(3)	C(55)	42.9 (4)	W(3)	W(4)	N(54)	93.1 (4)
W(3)	W(1)	O(41)	46.0 (3)	W(2)	W(3)	W(4)	58.6 (1)	W(3)	W(4)	C(55)	51.7 (4)
W(3)	W(1)	O(45)	88.2 (3)	W(2)	W(3)	O(21)	96.5 (3)	O(29)	W(4)	O(33)	88.8 (4)
W(3)	W(1)	C(55)	53.1 (4)	W(2)	W(3)	O(25)	136.6 (3)	O(29)	W(4)	O(37)	168.3 (4)
W(4)	W(1)	O(5)	101.7 (3)	W(2)	W(3)	O(37)	91.2 (3)	O(29)	W(4)	O(45)	84.3 (4)
W(4)	W(1)	O(9)	158.9 (3)	W(2)	W(3)	O(41)	132.8 (3)	O(29)	W(4)	N(54)	93.8 (4)
W(4)	W(1)	O(41)	89.5 (3)	W(2)	W(3)	O(49)	47.8 (3)	O(29)	W(4)	C(55)	87.2 (5)
W(4)	W(1)	O(45)	48.9 (2)	W(2)	W(3)	C(55)	43.6 (4)	O(33)	W(4)	O(37)	84.8 (4)
W(4)	W(1)	C(55)	52.5 (4)	W(4)	W(3)	O(21)	144.4 (3)	O(33)	W(4)	O(45)	89.3 (4)
O(5)	W(1)	O(9)	89.8 (4)	W(4)	W(3)	O(25)	129.5 (3)	O(33)	W(4)	N(54)	93.5 (5)
O(5)	W(1)	O(41)	157.7 (4)	W(4)	W(3)	O(37)	46.5 (3)	O(33)	W(4)	C(55)	175.6 (5)
O(5)	W(1)	O(45)	90.4 (4)	W(4)	W(3)	O(41)	90.6 (3)	O(37)	W(4)	O(45)	85.9 (4)
O(5)	W(1)	C(55)	103.2 (5)	W(4)	W(3)	O(49)	88.8 (3)	O(37)	W(4)	N(54)	96.3 (4)
O(9)	W(1)	O(41)	86.0 (4)	W(4)	W(3)	C(55)	51.4 (4)	O(37)	W(4)	C(55)	99.0 (5)
O(9)	W(1)	O(45)	149.9 (4)	O(21)	W(3)	O(25)	86.1 (5)	O(45)	W(4)	N(54)	176.6 (4)
O(9)	W(1)	C(55)	107.9 (5)	O(21)	W(3)	O(37)	169.1 (4)	O(45)	W(4)	C(55)	88.8 (5)
O(41)	W(1)	O(45)	82.5 (4)	O(21)	W(3)	O(41)	90.1 (5)	N(54)	W(4)	C(55)	88.4 (5)
O(41)	W(1)	C(55)	98.9 (5)	O(21)	W(3)	O(49)	91.2 (5)	W(1)	O(5)	C(6)	149.4 (10)
O(45)	W(1)	C(55)	101.3 (5)	O(21)	W(3)	C(55)	93.0 (5)	W(1)	O(9)	C(10)	133.6 (9)
W(3)	W(2)	W(4)	60.2 (1)	O(25)	W(3)	O(37)	83.0 (4)	W(2)	O(13)	C(14)	134.0 (9)
W(3)	W(2)	O(13)	115.4 (3)	O(25)	W(3)	O(41)	90.3 (4)	W(2)	O(17)	C(18)	134.0 (10)
W(3)	W(2)	O(17)	146.8 (3)	O(25)	W(3)	O(49)	88.9 (4)	W(3)	O(21)	C(22)	137.4 (10)
W(3)	W(2)	O(49)	45.3 (3)	O(25)	W(3e	C(55)	179.2 (5)	W(3)	O(25)	C(26)	131.7 (9)
W(3)	W(2)	N(54)	93.6 (3)	O(37)	W(3)	O(41)	90.3 (4)	W(4)	O(29)	C(30)	126.2 (9)
W(3)	W(2)	C(55)	52.5 (4)	O(37)	W(3)	O(49)	88.2 (5)	W(4)	O(33)	C(34)	137.9 (10)
W(4)	W(2)	O(13)	164.6 (3)	O(37)	W(3)	C(55)	97.8 (5)	W(3e	O(37)	W(4)	86.2 (4)
W(4)	W(2)	O(17)	107.7 (3)	O(41)	W(3)	O(49)	178.5 (5)	W(3)	O(37)	C(38)	138.8 (9)
W(4)	W(2)	O(49)	88.4 (3)	O(41)	W(3)	C(55)	89.6 (5)	W(4)	O(37)	C(38)	134.2 (9)
W(4)	W(2)	N(54)	46.2 (4)	O(49)	W(3)	C(55)	91.2 (5)	W(1)	O(41)	W(3)	87.0 (3)
W(4)	W(2)	C(55)	53.8 (4)	W(1)	W(4)	W(2)	87.1 (1)	W(1)	O(41)	C(42)	137.9 (8)
O(13)	W(2)	O(17)	83.7 (4)	W(1)	W(4)	W(3)	59.9 (0)	W(3)	O(41)	C(42)	134.2 (8)
O(13)	W(2)	O(49)	79.9 (4)	W(1)	W(4)	O(29)	85.1 (3)	W(1)	O(45)	W(4)	85.0 (3)
O(13)	W(2)	N(54)	123.4 (5)	W(1)	W(4)	O(33)	135.4 (3)	W(1)	O(45)	C(46)	128.3 (8)
O(13)	W(2)	C(55)	137.4 (5)	W(1)	W(4)	O(37)	92.7 (3)	W(4)	O(45)	C(46)	128.7 (8)
O(17)	W(2)	O(49)	163.5 (4)	W(1)	W(4)	O(45)	46.2 (3)	W(2)	O(49)	W(3)	87.0 (5)
O(17)	W(2)	N(54)	97.7 (5)	W(1)	W(4)	N(54)	131.0 (4)	W(2)	O(49)	C(50)	135.6 (9)
O(17)	W(2)	C(55)	94.8 (5)	W(1)	W(4)	C(55)	42.6 (4)	W(3)	O(49)	C(50)	136.8 (9)
O(49)	W(2)	N(54)	91.1 (5)	W(2)	W(4)	W(3)	61.2 (0)	W(2)	N(54)	W(4)	89.4 (5)
O(49)	W(2)	C(55)	97.5 (5)	W(2)	W(4)	O(29)	97.3 (3)	W(2)	N(54)	C(53)	129.0 (11)
N(54)	W(2)	C(55)	99.1 (6)	W(2)	W(4)	O(33)	137.6 (3)	W(4)	N(54)	C(53)	140.9 (11)
W(1)	W(3)	W(2)	85.9 (1)	W(2)	W(4)	O(37)	94.0 (3)	W(1)	C(55)	W(2)	163.5 (8)
W(1)	W(3)	W(4)	60.4 (1)	W(2)	W(4)	O(45)	133.0 (3)	W(1)	C(55)	W(3)	84.0 (5)
W(1)	W(3)	O(21)	95.7 (4)	W(2)	W(4)	N(54)	44.4 (4)	W(1)	C(55)	W(4)	84.9 (5)
W(1)	W(3)	O(25)	137.1 (3)	W(2)	W(4)	C(55)	44.8 (4)	W(2)	C(55)	W(3)	83.9 (5)
W(1)	W(3)	O(37)	92.5 (3)	W(3)	W(4)	O(29)	138.0 (3)	W(2)	C(55)	W(4)	81.5 (5)
				W(3)	W(4)	O(33)	132.1 (3)	W(3)	C(55)	W(4)	77.0 (4)

the $6a_1$ W–C bonding orbital that lies very low in energy (ca. 29 eV) and is not shown in Figure 3. Despite the large energetic separation between carbon 2s and frontier a_1 orbitals the interaction is sizable due to very large overlap between C 2s and $W_4(OH)_{13}^{3-}$ fragments.

The utility of our fragment formalism is that the converged results of $W_4(OH)_{13}C^+$ can be transformed into a basis consisting of the canonical orbitals of the $W_4(OH)_{13}^{3-}$ cluster fragment and carbon atomic orbitals. The advantages of this approach are that it allows (1) for the construction of the fragment orbital correlation diagram from the diagonal Fock matrix elements in the transformed basis, (2) for the examination of the Mulliken populations of the canonical valence orbitals as a result of W–C bonding,[17] and, most important, (3) for the assessment of fragment orbital interactions between $W_4(OH)_{13}^{3-}$ and C^{4+} fragments on an orbital by orbital basis. In Table V are listed the important fragment orbital overlap populations between $W_4(OH)_{13}^{3-}$ and C^{4+} fragments. The table complements the important features of the correlation diagram in Figure 3 and reveals those fragment orbitals of $W_4(OH)_{13}^{3-}$ that have significant orbital overlap populations with carbon atomic orbitals. The b_1 and b_2 fragment interactions are very straightforwrd, and Table V demonstrates that the primary interaction of the b_1 C 2p orbital is with $16b_1$ cluster fragment, and the b_2 C 2p orbital interaction is with the $13b_2$ cluster fragment. From the correlation diagram one can see a dramatic destabilization of $16b_1$ and $13b_2$ $W_4(OH)_{13}^{3-}$ cluster fragment orbitals that result from bonding interactions with C 2p atomic orbitals. The interaction of C 2s and C 2p a_1 atomic orbitals with a_1 cluster fragment orbitals is much more complicated and Table V shows that the $17a_1$, $18a_1$, and $19a_1$ $W_4(OH)_{13}^{3-}$

Table V. Fragment Orbital Overlap Populations between $W_4(OH)_{13}^{3-}$ and C^{4+} Fragment Orbitals

$17a_1$–C 2s	0.143	$13b_2$–C 2p	0.483
$18a_1$–C 2s	0.280	$14b_2$–C 2p	0.020
$19a_1$–C 2s	0.079	$17a_1$–C 2p	0.163
$16b_1$–C 2p	0.617	$19a_1$–C 2p	0.324

(17) This is essentially an application of the "clusters in molecules" formalism that has been successfully used in the understanding of metal–metal and metal–ligand bonding trends in transition-metal cluster compounds. See, for example: (a) Bursten, B. E.; Cotton, F. A.; Hall, M. B.; Najjar, R. C. *Inorg. Chem.* **1982**, *21*, 302. (b) Chisholm, M. H.; Cotton, F. A.; Fang, A.; Kober, E. M. *Inorg. Chem.* **1984**, *23*, 749. (c) Cotton, F. A.; Fang, A. *J. Am. Chem. Soc.* **1982**, *104*, 113. (d) Bursten, B. E.; Chisholm, M. H.; Clark, D. L., manuscript in preparation.

Table VI. Selected Mulliken Populations of the Canonical Orbitals of $W_4(OH)_{13}^{3-}$ in $W_4(OH)_{13}C^+$

orbital	$W_4(OH)_{13}^{3-}$	$W_4(OH)_{13}C^+$
$13b_1$	2.000	1.996
$10b_2$	2.000	1.989
$8a_2$	2.000	1.996
$9a_2$	2.000	1.997
$14b_1$	2.000	1.996
$16a_1$	2.000	1.954
$11b_2$	2.000	1.989
$15b_1$	2.000	1.993
$10a_2$	2.000	1.995
$17a_1$	2.000	1.163 (C 2s, C $2p_z$)
$12b_2$	2.000	1.907 (M–M)
$18a_1$	2.000	1.261 (C 2s)
$11a_2$	2.000	1.993 (M–M)
$16b_1$	2.000	0.785 (C $2p_x$)
$19a_1$	2.000	0.699 (C 2s, C $2p_z$)
$13b_2$	2.000	0.674 (C $2p_y$)
$14b_2$	0.000	0.046 (C $2p_y$)
$12a_2$	0.000	0.009
$15b_2$	0.000	0.019
$20a_1$	0.000	0.036
$21a_1$	0.000	0.019
$17b_1$	0.000	0.012
$16b_2$	0.000	0.015
C 2s	0.000	1.643
C $2p_x$	0.000	1.228
C $2p_y$	0.000	1.363
C $2p_z$	0.000	1.292

cluster fragment orbitals all have strong interactions with C a_1 atomic orbitals. In the delocalized molecular orbital picture it is not possible to trace all of this a_1 W–C bonding to a single molecular orbital. However, the $19a_1$ oribtal's primary interaction is with the a_1 C 2p atomic orbital resulting in the $14a_1$ and $21a_1$ orbitals of $W_4(OH)_{13}C^+$. The $17a_1$ and $18a_1$ oribtals undergo a rehybridization as a result of interaction with both C 2s and C 2p atomic orbitals, and most important is the observation that the carbon 2s orbital has significant overlap with the $W_4(OH)_{13}^{3-}$ fragment.

The above observations are further amplified by examination of selected Mulliken populations of the canonical valence orbitals of the $W_4(OH)_{13}^{3-}$ fragment in the $W_4C(OH)_{13}^+$ molecule listed in Table VI. The first nine populations listed in Table VI tell the same story as the correlation diagram in Figure 3, namely, that the "block" of metal–ligand bonding and oxygen lone-pair orbitals of $W_4(OH)_{13}^{3-}$ are essentially unperturbed by interaction with carbon to form $W_4C(OH)_{13}^+$. This is revealed in Table VI via the relatively unchanged Mulliken population of these orbitals of $W_4(OH)_{13}^{3-}$ in $W_4C(OH)_{13}^+$ as each remains essentially doubly occupied in $W_4C(OH)_{13}^+$. Similarly, it can be seen in the populations that the $12b_2$ and $11a_2$ metal–metal cluster bonding orbitals remain fully occupied and are unperturbed by interaction with carbon to form $W_4C(OH)_{13}^+$. By contrast, the $17a_1$, $18a_1$, $16b_1$, $19a_1$, and $13b_2$ orbitals of $W_4(OH)_{13}^{3-}$ that all have significant overlap with carbon (Table V) are all depopulated as a result of W–C bonding. This illustrates a very important point. Strong covalent W–C bonding interactions result in a mixing of metal–metal and metal–carbon bonding such that occupation of W–C bonding orbitals also contributes to the overall metal–metal cluster bonding. This reemphasizes our original comment that it is only a formalism in electron counting that arrives at six electrons for metal–metal cluster bonding. The Mulliken populations clearly show that the carbido carbon atom adds electron density to metal–metal cluster bonding and, in a way, provides extra "molecular glue" to hold the cluster together.

Table VII. Atomic Orbital Overlap Populations[a] between Carbon and Tungsten for $W_4(OH)_{13}C^+$

	W_w[b]	W_b[c]
C(2s)–W(d)	0.161	0.019
C($2p_x$)–W(d)	0.150	0.070
C($2p_y$)–W(d)	0.156	0.005
C($2p_z$)–W(d)	0.154	0.011
C(2s)–W(dsp)	0.136	0.021
C($2p_x$)–W(dsp)	0.149	0.137
C($2p_y$)–W(dsp)	0.212	−0.015
C($2p_z$)–W(dsp)	0.149	0.057
total C(p)–W(dsp)	0.510	0.179
total C(sp)–W(dsp)	0.646	0.200

[a] The designation C(2s)–W(d) represents the total atomic orbital overlap population between the C 2s atomic orbital and all five W 5d atomic orbitals. C(2s)–W(dsp) represents the total atomic orbital overlap population between C 2s atomic orbital and all nine valence atomic orbitals of the W atom (5d, 1s, 3p) etc. [b] Wingtip. [c] Backbone.

A very impressive feature of Figure 3 is that interaction of the $W_4(OH)_{13}^{3-}$ cluster with carbon dramatically stabilizes the cluster by opening up the HOMO–LUMO gap that as calculated by the Fenske–Hall method is 3.65 eV, remarkably large for a cluster of this size.

Let us now take a more detailed look at the nature of metal–metal and metal–carbon bonding. In our model cluster of formula $W_4(OH)_{13}C^+$ we have a formal W_4^{18+} core, and as such, the six electrons of tungsten occupy the $11a_2$, $19a_1$, and $13b_2$ metal–metal bonding orbitals as indicated in Figure 3. These three metal–metal cluster bonding orbitals are illustrated qualitatively in I. The $13b_2$

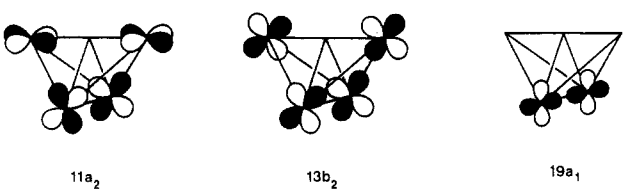

I

orbital is metal–metal bonding between the wingtip and backbone tungsten atoms and is delocalized across the faces and edges of the triangles formed by backbone and wingtip tungsten atoms. The $19a_1$ orbital is concentrated between backbone tungsten atoms with virtually no wingtip contribution while the $11a_2$ orbital is localized along the four edges of the butterfly and with bonding between wingtip and backbone atoms.

The tungsten–carbon bonding is primarily localized to the $6a_1$, $7b_2$, $14a_1$, and $12b_1$ molecular orbitals of $W_4(OH)_{13}C^+$ that are illustrated qualitatively in II along with

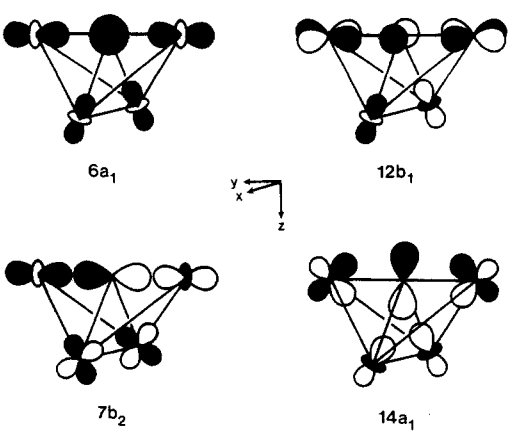

II

a coordinate system for the molecule. The C 2s orbital interacts primarily with wingtip tungsten atoms but does have a small interaction with the backbone atoms and results in formation of the $6a_1$ W–C σ-bonding orbital shown qualitatively in II. The C $2p_y$ orbital interacts solely with the wingtip atoms resulting in a strong W–C σ bonding $7b_2$ orbital, and it can be seen in II that the $7b_2$ orbital does have a contribution from the backbone tungsten atoms, but their interaction with carbon is negligible. The C $2p_x$ and C $2p_z$ orbitals are both involved in σ interactions with the backbone tungsten atoms and π interactions with the wingtip tungsten atoms, and the resulting $12b_1$ and $14a_1$ bonding orbitals (respectively) are also illustrated schematically in II. The magnitudes of the wingtip and backbone W–C bonding interactions are reflected in the W–C atomic orbital overlap populations listed in Table VII. It can be seen from Table VII that the largest overlap population involving W d atomic orbitals occurs between the C 2s and wingtip W d orbitals. Similarly, the overlap between C $2p_x$, $2p_y$, and $2p_z$ atomic orbitals with wingtip W d atomic orbitals are all of comparable magnitude yet significantly larger than any overlap between backbone tungsten and carbon atomic oribtals. When the interactions of virtual tungsten s and p atomic orbitals are taken into account, the net result is that the total C(sp)–W(dsp) overlap population is on the order of 3 times larger for the wingtip than backbone tungsten atoms. Although overlap population can be only taken as an approximate measure of bond strength, the large differences in values for wingtip and backbone tungsten atoms attest to the importance of the interaction of both C 2s and 2p atomic orbitals with wingtip tungsten atoms. This situation is very similar to that observed by Harris and Bradley[14] in their studies of the somewhat related Fe_4C clusters with the notable exception of the lack of involvement of C 2s atomic orbitals in metal–carbon bonding in the latter.

The important W–C bonding interactions in $W_4C(OH)_{13}^+$ can be accentuated with the aid of selected contour plots taken through the molecular *xz* or *yz* planes that are defined in III. The *xz* and *yz* planes shown in III each

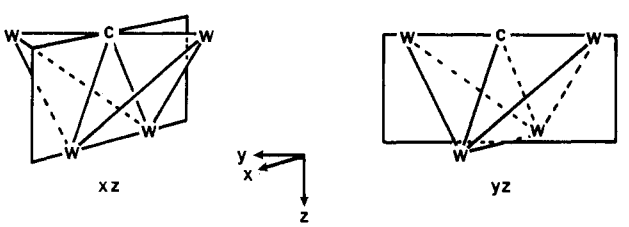

III

contain the carbido carbon atom and either the backbone (*xz*) or wingtip (*yz*) tungsten atoms respectively. Contour plots taken in the *xz* or *yz* planes can thus be used to illustrate the interaction of the carbido carbon atom with backbone or wingtip tungsten atoms. In Figure 4 we illustrate the W–C bonding interaction of the $14a_1$ orbital through the use of contour plots, and these plots can be compared to the schematic illustrations shown in II. The interaction between carbido carbon and wingtip tungsten atoms in the $7b_2$ orbital is illustrated with a contour plot in the *yz* plane in Figure 5 and may also be compared to the illustrations in II. Finally, the W–C bonding interactions in the $6a_1$ orbital of $W_4C(OH)_{13}^+$ are illustrated with contour plots in Figure 6 and can be compared to the schematic drawing of the $6a_1$ orbital in II.

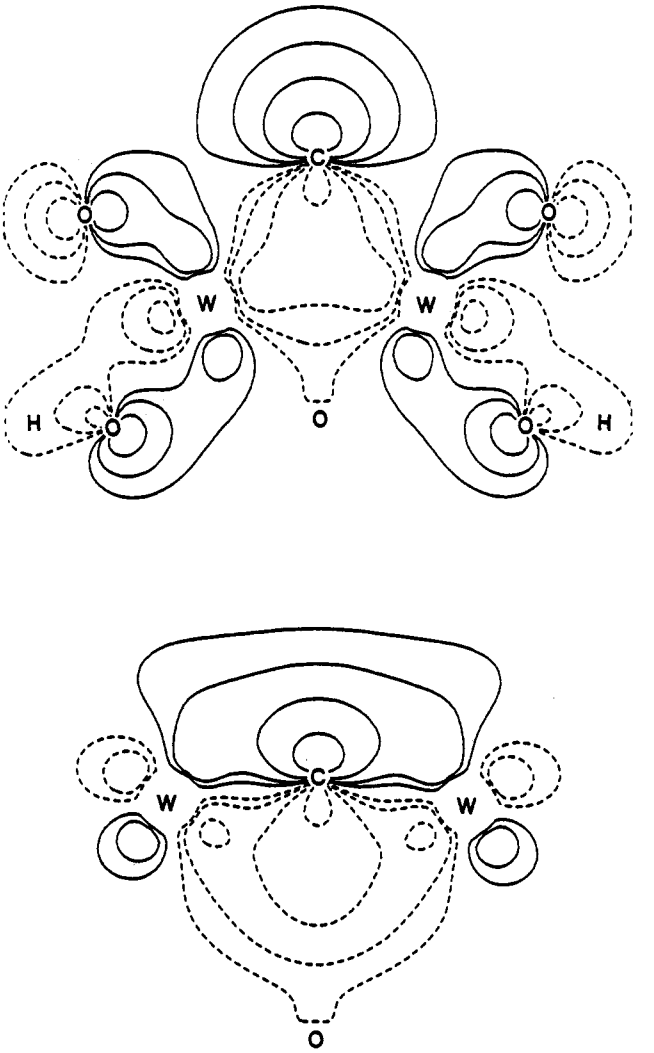

Figure 4. Contour plots of the $14a_1$ W–C bonding orbital of $W_4(C)(OH)_{13}^+$ taken as a slice through the *xz* (top) and *yz* (bottom) planes defined in the text. The *xz* plane illustrates the σ interaction with the backbone W atoms, and the *yz* plane illustrates the π interaction with the wingtip W atoms. Dashed lines represent negative wave function values, and solid lines represent positive values. Contour values are ±0.02, ±0.04, ±0.08, and ±0.16 e/A^3 in this and all subsequent plots.

The Remarkable Similarity in Electronic and Molecular Structures of High- and Low-Valent Tetranuclear Butterfly Carbido Cluster Compounds. Now that the electronic structure and bonding in $W_4C(OH)_{13}^+$ has been addressed, we note some rather fascinating similarities and differences in *both* metal–metal and metal–carbon bonding between our early-transition-metal, high-valent cluster carbide of formula $W_4C(OH)_{13}^+$ and the late-transition-metal, low-valent cluster carbides of formula $Fe_4C(CO)_{13}$,[12] $Fe_4C(CO)_{12}^{2-}$,[18] $Fe_4C(CO)_{12}(CO_2Me)^-$,[19] and $Fe_4C(CO)_{12}H^-$.[20] These latter "iron butterfly" carbido clusters have been the subject of recent theoretical studies of two groups: Harris and Bradley (HB)[14] and Wijeyesekera, Hoffmann, and Wilker (WHW).[15,16] Both groups have independently shown via different computational techniques that in a very simplified view, the primary metal–metal and metal–carbon σ bonding in Fe_4C clusters occurs through interaction of carbon atomic orbitals and

(18) Davis, J. H.; Beno, M. A.; Williams, J. M.; Zimmie, J. A.; Tachikawa, M.; Muetterties, E. L. *Proc. Natl. Acad. Sci. U.S.A.* **1981**, *78*, 668.
(19) Bradley, J. S.; Ansell, G. B.; Hill, E. W. *J. Am. Chem. Soc.* **1979**, *10*, 7417.
(20) Holt, E. M.; Whitmire, K. W.; Schriver, D. F. *J. Organomet. Chem.* **1981**, *213*, 125.

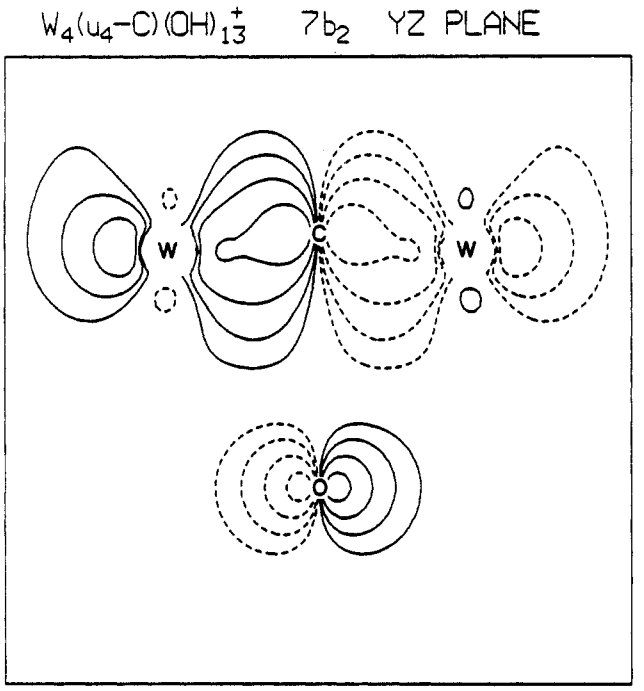

Figure 5. Contour plot of the $7b_2$ W–C bonding orbital of $W_4(C)(OH)_{13}^+$ taken as a slice through the *yz* plane defined in the text and emphasizing the σ interaction between wingtip W atoms and C 2p atomic orbitals.

frontier "e_g" orbitals of the Fe_4 cluster fragments. In this simplified description, there is essentially no net Fe–Fe bonding between Fe_4 cluster framework "t_{2g}" orbitals because the levels containing both the bonding and antibonding interactions between these orbitals are occupied. Thus the "t_{2g}" orbitals give rise to a very narrow nonbonding d band in these Fe_4C clusters, and metal–metal and metal–carbon σ bonding occurs through the "e_g" orbitals. This is because the local geometry about each $Fe(CO)_3$ group is octahedral such that the carbido carbon atom and two adjacent Fe atoms occupy the three missing vertices of an octahedron. Thus in the Fe_4C clusters, the Fe–Fe and Fe–C σ bonding takes place via "e_g" orbitals.

In the W_4C cluster, wingtip and backbone W atoms have local square-based-pyramidal WO_4C or octahedral WO_5C geometries; i.e., the carbido C atom occupies a vertex of the octahedral fragment. As a result, W–C bonding, like Fe–C bonding, utilizes "e_g" orbital interactions for W–C σ bonding. By contrast, W–W bonding in the W_4C clusters takes place through the "t_{2g}" orbitals as compared to the "e_g" Fe–Fe bonding in Fe_4C clusters. The overall metal–carbon bonding in W_4C and Fe_4C clusters is therefore very similar. Since the carbido C atom occupies a vertex of an octahedron, the metal–carbon σ bonding utilizes "e_g" orbitals and the metal–carbon π interactions employ "t_{2g}" orbitals. The metal–metal bonding in W_4C clusters uses "t_{2g}" orbitals while "e_g" orbitals are used in Fe_4C clusters. This fundamental difference in metal–metal bonding between high- and low-valent cluster carbides arises from what we will refer to as a d^3–d^9 "hole formalism" that can be illustrated through the use of C_{3v} ML_3 fragments. While the Fe_4C clusters are constructed from C_{3v} $Fe(CO)_3$ fragments, it is important to recognize that the W_4C clusters are *not* constructed from C_{3v} $W(OR)_3$ fragments. We simply introduce a comparison of C_{3v} ML_3 fragments here as a pedagogical aid for understanding the fundamental difference in metal–metal bonding between high- and low-valent cluster carbides.

The frontier orbitals of a C_{3v} ML_3 fragment are well-known[21] and consist of a low-lying $1a_1$ + 1e, remnants of

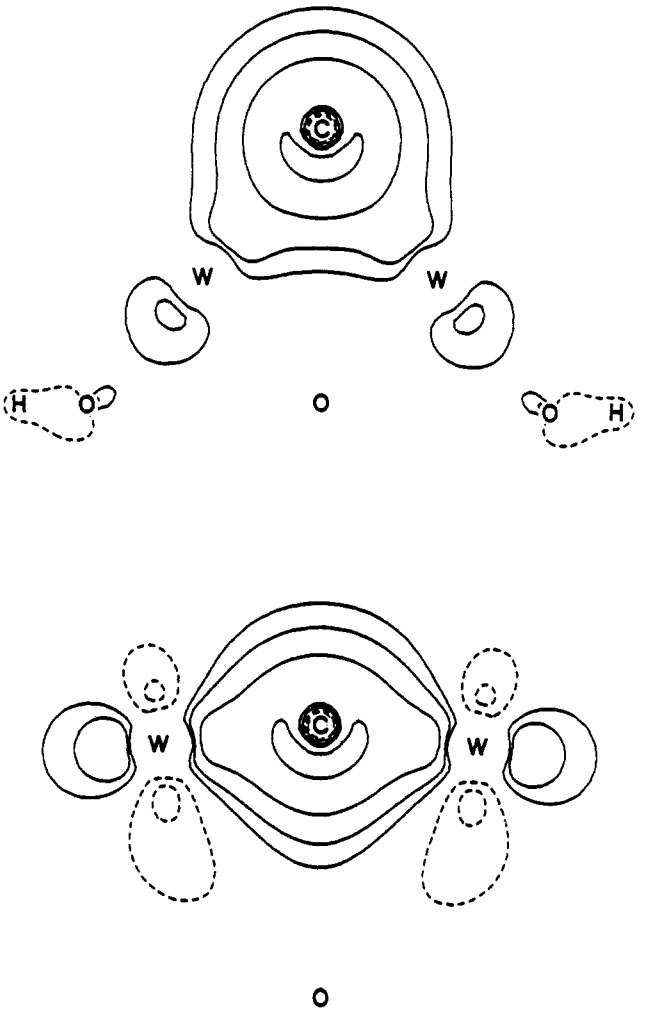

Figure 6. Contour plots of the $6a_1$ W–C bonding orbital of $W_4(C)(OH)_{13}^+$ taken as a slice through the *xz* (top) and *yz* (bottom) planes defined in the text.

the octahedral t_{2g} set, and a high-lying $2a_1$ + 2e. The $2a_1$ oribital is a "dsp" hybrid, and the 2e orbital is a remnant of the octahedral e_g set. In a d^3 $W(OR)_3$ fragment, the three valence electrons reside in the lower t_{2g} set, while in a d^9 $Fe(CO)_3^-$ fragment, the three valence electrons reside in the upper e_g set, yet the two octahedral fragments are isolobal via a d^3–d^9 "hole formalism" as indicated in IV.

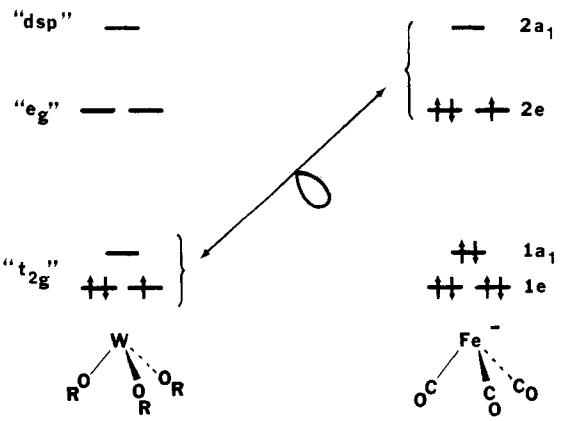

IV

(21) (a) Elian, M.; Hoffmann, R. *Inorg. Chem.* **1975**, *14*, 1058. (b) Elian, M.; Chen, M. M. L.; Mingos, D. M. P.; Hoffmann, R. *Inorg. Chem.* **1976**, *15*, 1148. (c) Albright, T. A.; Hofmann, P.; Hoffmann, R. *J. Am. Chem. Soc.* **1977**, *99*, 7546.

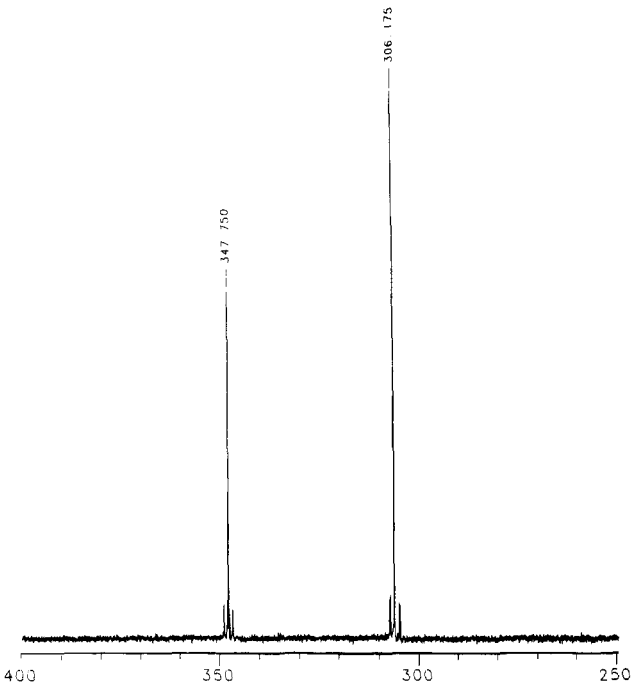

Figure 7. $^{13}C\{^1H\}$ NMR spectrum of a crystalline sample of $W_4(*CO)_2(O\text{-}i\text{-}Pr)_{12}$ and [A] in toluene-d_8 solution at 75 MHz and 22 °C.

Clearly the W_4C cluster carbide is not constructed of C_{3v} $W(OR)_3$ fragments due in part to the propensity for alkoxy group bridge formation, but the fundamental essence of metal–metal bonding through t_{2g} or e_g orbitals in W_4C and Fe_4C clusters (respectively) is contained within this simple pedagogical comparison. In this fashion it is easy to see why $W_4C(OH)_{13}^+$, $Fe_4C(CO)_{13}$, $Fe_4C(CO)_{12}H^-$, and $Fe_4C(CO)_{12}^{2-}$ all have essentially six electrons in a_2, b_2, and a_1 metal–metal cluster bonding orbitals even though the W_4C cluster uses "t_{2g}" orbitals and the Fe_4C clusters use "e_g" orbitals to form the metal–metal cluster bonds. In a similar fashion, the metal–carbon bonding is essentially identical between W_4C and Fe_4C clusters, and indeed, the a_1, b_1, and b_2 metal–carbon bonding orbitals in II show a striking similarity to those observed by HB[14] and WHW[15,16] in the Fe_4C clusters. There is, however, one noticeable difference in the magnitude of C 2s atomic orbital participation to M–C bonding as calculated by the Fenske–Hall method. As noted previously, the largest atomic orbital overlap population of ca. 0.16 (Table VII) occurs between wingtip W d orbitals and the C 2s orbital. By comparison, the overlap population between C 2s and wingtip Fe d orbitals in $Fe_4C(CO)_{12}^{2-}$ is a mere 0.04 on the basis of Fenske–Hall results.[22] Clearly, the larger radial extension of the W 5d orbital relative to the smaller Fe 3d orbital results in a substantially larger overlap with the low-lying C 2s orbital. From simple perturbation theory, the larger overlap leads directly to a larger interaction. We feel that this increased C 2s participation in W_4C bonding is reflected in the magnitude of the ^{183}W–^{13}C coupling constants in a related W_4C cluster discussed in the next section.

Attempted Synthesis of $W_4(C)(O)(O\text{-}i\text{-}Pr)_{12}$. Following our earlier studies on the stepwise reduction of C≡O by W≡W bonds supported by alkoxide ligands:[23,24] W≡W + C≡O → (W═W)(μ-C═O) → [(W—W)(μ-C-O)]$_2$, we have tried to form the carbido–oxo compounds $W_4(C)(O)(O\text{-}i\text{-}Pr)_{12}$ in two reactions outlined in eq 2 and 3.

$$W_4(\mu\text{-}CO)_2(O\text{-}i\text{-}Pr)_{12} + 2W_2(O\text{-}t\text{-}Bu)_6 \xrightarrow[\text{hexane}/i\text{-PrOH}]{25\ ^\circ C} [A] \quad (2)$$

$$W_2(O\text{-}t\text{-}Bu)_6(\mu\text{-}CO) + W_2(O\text{-}t\text{-}Bu)_6 \xrightarrow[\text{hexane}/i\text{-PrOH}]{25\ ^\circ C} W_4(\mu\text{-}CO)_2(O\text{-}i\text{-}Pr)_{12} + [A] \quad (3)$$

In both reactions we are trying to take advantage of coordinative unsaturation about the metal centers and the reducing power of the $(W{\equiv}W)^{6+}$ unit, introduced as $W_2(O\text{-}t\text{-}Bu)_6$ but transformed to $W_2(O\text{-}i\text{-}Pr)_6$ upon alcoholysis.[25] The simple addition of *i*-PrOH (excess) to $W_2(O\text{-}t\text{-}Bu)_6(\mu\text{-}CO)$ in hexane provides the general synthesis of $W_4(\mu\text{-}CO)_2(O\text{-}i\text{-}Pr)_{12}$ whose structure is diagramatically shown in V.

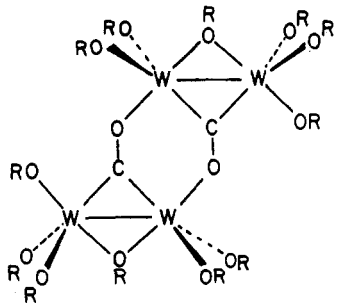

V

These reactions shown in eq 2 and 3 have been monitored by ^{13}C NMR spectroscopy employing *C≡O where *C represents 99 mol % ^{13}C. The ^{13}C NMR spectra of these reaction mixtures show only two ^{13}C signals in the region of interest and are assignable to the *C atoms. The spectrum of one such reaction mixture is shown in Figure 7. The signal at ca. δ 306 is assignable to that of $W_4(\mu\text{-}*CO)_2(O\text{-}i\text{-}Pr)_{12}$ (by comparison with authentic samples) and reveals the presence of two couplings to ^{183}W nuclei, ^{183}W, $I = {}^1/_2$, 14.5% natural abundance. The large magnitude of those couplings ca. 180 Hz is consistent with the alkylidyne character of the carbon-to-tungsten bonds: W–C distances are ca. 1.95 Å.[23,24] The spectrum of the new compound [A] in reactions 2 and 3 is shown in Figure 8. The resonance at ca. δ 350 shows coupling to four inequivalent nuclei, two with large couplings to ^{183}W, 160 and 177 Hz, and two with small couplings, 24 and 37 Hz. Bearing in mind the isoelectronic nature of oxo and imido (NR) ligands, we would like to propose that compound [A] is $W_4(C)(O)(O\text{-}i\text{-}Pr)_{12}$ having a structure related to the imido one reported here by the mere substitution of O for NMe. We have not yet been able to separate [A] from the mixture of products formed in reactions 2 and 3 that include in addition to [A], $W_4(\mu\text{-}CO)_2(O\text{-}i\text{-}Pr)_{12}$ and $W_4(O\text{-}i\text{-}Pr)_{12}$. Further work aimed at a logical synthesis of [A] and related $W_4(C)(NR)(O\text{-}i\text{-}Pr)_{12}$ is in progress. We merely introduce the ^{13}C NMR spectrum of [A] since it fits exactly our expectations on the basis of the imido–carbido structure reported here. Note the large couplings are expected to the wingtip tungsten atoms and the small couplings to the backbones. The presence of an oxo (or imido) bridge renders all four tungsten nuclei inequivalent, but the

(22) Harris, S., personal communication.
(23) Chisholm, M. H.; Hoffman, D. M.; Huffman, J. C. *Organometallics* **1985**, *4*, 986.
(24) Blower, P. J.; Chisholm, M. H.; Clark, D. L.; Eichhorn, B. W. *Organometallics* **1986**, *5*, 2125.
(25) The equilibrium $2W_2(O\text{-}i\text{-}Pr)_6 \rightleftharpoons W_4(O\text{-}i\text{-}Pr)_{12}$ has recently been noted: Chisholm, M. H.; Clark, D. L.; Folting, K.; Huffman, J. C. *Angew. Chem., Int. Ed. Engl.* **1986**, *25*, 1014.

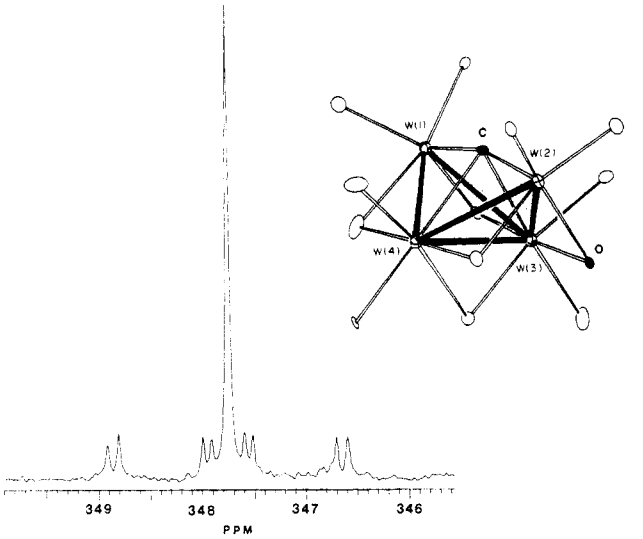

Figure 8. Expanded view of the $^{13}C\{^1H\}$ NMR spectrum of [A] in toluene-d_8 solution at 75 MHz and 22 °C. Proposed structure of [A] is shown in inset.

general pairwise relationship of wingtip and backbone tungsten to carbon bonds remain. The magnitude of the coupling constants parallels the bond distances and also reflects the significant C 2s orbital contributions to the W–C bonding noted previously.

Concluding Remarks

We believe our fortuitous discovery of the compound $W_4(C)(NMe)(O\text{-}i\text{-}Pr)_{12}$ represents the first of a potentially large class of carbido tungsten clusters supported by alkoxide ligands. The bonding and reactivity of these compounds should prove a fascinating topic for future research both as models of carbido metal oxide species and with respect to $M_4(\mu_4\text{-}C)$ carbonyl-supported compounds.

Experimental and Computational Procedures

Computational Procedures. We have employed a model system of formula $W_4C(OH)_{13}^+$ that was idealized to C_{2v} point symmetry by using averaged W–O and W–C distances from the crystal structure of $W_4C(NMe)(O\text{-}i\text{-}Pr)_{12}$ with an eye toward removing the distortions due to the presence of the NMe ligand. The backbone W–W distance used was 2.800 Å, and the four edges of the W_4 butterfly used W–W distances of 2.811 Å. The W–C distances used were 1.910 and 2.250 Å for wingtip and backbone tungsten atoms, respectively. Wingtip–terminal and –bridging W–O distances were averaged to 1.890 and backbone–terminal and –bridging W–O distances were averaged to 1.910 and 2.020 Å, respectively, except for the terminal W–O bonds trans to C, where 2.010 Å was used. The O atom bridging the backbone of the butterfly used a W–O distance of 2.040 Å, and the O–H distance was assumed to be 0.96 Å.

Molecular orbital calculations were performed by using the method of Fenske and Hall that has been described in detail elsewhere[13] and its applications reviewed.[26] The Fenske–Hall method is an approximate Hartree–Fock Roothaan SCF–LCAO procedure, and the final results depend only upon the chosen atomic basis set and internuclear distances. SCF calculations were performed in the atomic basis on the $W_4(OH)_{13}^{3-}$ fragment and the $W_4C(OH)_{13}^+$ cluster. Following convergence, the results of $W_4C(OH)_{13}^+$ were transformed into a basis consisting of the canonical fragment orbitals of $W_4(OH)_{13}^{3-}$ and C atomic orbitals. All the calculations described in this paper were obtained at the Indiana University Computational Chemistry Center using a VAX 11/780 computer system. Contour plots were generated on a TALARIS 800 laser printer with solid lines representing positive density contours and dashed lines representing negative density contours.

All atomic wave functions were generated by a best fit to Herman–Skillman atomic calculations using the method of Bursten, Jensen, and Fenske.[27] Contracted double-ζ representations were used for the W 5d as well as C and O 2p AO's. Basis functions for the metal atom were derived for a +1 oxidation state with the valence s and p exponents fixed at 1.8 for W 6s and 6p orbitals. An exponent of 1.16 was used for the H 1s atomic orbital since this value minimizes the energy for methane.[28]

Physical Techniques. ^1H NMR spectra were recorded on a Nicolet NT-360 spectrometer at 360 MHz in dry and oxygen-free toluene-d_8 or benzene-d_6. All ^1H NMR chemical shifts are reported in parts per million relative to the CHD_2 quintet of toluene-d_8 set a δ 2.09 or the ^1H impurity in benzene-d_6 set at δ 7.15. ^{13}C NMR spectra were recorded on a Nicolet NT-360 spectrometer at 90 MHz or on a Varian XL-300 spectrometer at 75 MHz in toluene-d_8. All ^{13}C NMR chemical shifts are reported in parts per million relative to the ipso carbon of toluene-d_8 set at δ 137.5. Infrared spectra were recorded on a Perkin-Elmer 283 spectrophotometer as Nujol mulls between CsI plates. Cyclic voltammograms were obtained with use of a Par 173 potentiostat, a Par 175 programmer, and a Houston 2000 X-Y recorder. Cyclic voltammetric studies employed a three-electrode, two-compartment cell and a platinum-disk electrode of nominal area 0.2 mm^2, probed by a luggin capillary. A pseudoreference electrode was employed consisting of a silver wire immersed in the supporting electrolyte solution inside the capillary, and a platinum gauze served as auxiliary electrode. No internal resistance compensation was used. All potentials quoted are at room temperature relative to SCE. A 0.2 M solution of tetra-*n*-butylammonium tetrafluoroborate ($[n\text{-}Bu_4N][BF_4]$) was employed as a supporting electrolyte,[29] and scan rates were 200 mV/s.

Synthesis. All reactions were carried out under an atmosphere of dry and oxygen-free nitrogen by using standard Schlenk and glovebox techniques. Hexane and toluene were degassed and eluted from a activated copper catalyst and molecular sieve columns and then stored over sieves and under nitrogen. THF and 1,2-dimethoxyethane were distilled from sodium benzophenone and stored under nitrogen and over sieves. *i*-PrOH was distilled from sodium metal (NaO-*i*-Pr) and stored under nitrogen and over sieves. Elemental analyses were performed by Alfred Bernhardt Microanalytishes Laboratorium, West Germany.

Synthesis of $W_4C(NMe)(O\text{-}i\text{-}Pr)_{12}$. Procedure I. (1) $W_2(NMe_2)_6$ (1.00 g, 1.58 mmol) was dissolved in hexane (10 mL) and *i*-PrOH (10 mL) was introduced via syringe. The yellow solution rapidly became brown and was then cooled to 0 °C. Brown cubes of $W_2(O\text{-}i\text{-}Pr)_6(HNMe_2)_2$ (ca. 30% yield) were obtained and removed by filtration. The volume of the filtrate was reduced and the solution cooled to 0 °C. Successive crystallizations yielded mixtures of the compounds $W_2(O\text{-}i\text{-}Pr)_6(HNMe_2)_2$, $W_4C(NMe)(O\text{-}i\text{-}Pr)_{12}$, and $W_4(O\text{-}i\text{-}Pr)_{12}$. Crystals of these compounds were separated by hand in a Vacuum Atmospheres Dri-Box. Earlier crystallizations were enriched in $W_2(O\text{-}i\text{-}Pr)_6(HNMe_2)_2$, while subsequent batches contained relatively more $W_4C(NMe)(O\text{-}i\text{-}Pr)_{12}$. The $W_4C(NMe)(O\text{-}i\text{-}Pr)_{12}$ obtained by this method was recrystallized from a solvent mixture of hexane and *i*-PrOH (1:1) at 0 °C. ^1H NMR (360 MHz, 22 °C, toluene-d_8): $\delta(OCHMe_2)$ 0.75–1.88 (72 H, overlapping doublets); $\delta(OCHMe_2)$ 4.38 (1 H, septet), 5.05 (2 H, septet), 5.29 (2 H, septet), 5.53 (1 H, septet), 5.65 (1 H, septet), 5.77 (1 H, septet), 5.83 (1 H, br), 6.12 (3 H, septet); $\delta(NMe)$ 4.98 (3 H, s). $^{13}C\{^1H\}$ NMR (75 MHz, 22 °C, toluene-d_8, at natural abundance ^{13}C): $\delta(OCHMe_2)$ 23–32 (overlapping singlets); $\delta(OCHMe_2)$ 70–84 (9 singlets of differing intensities); $\delta(NCH_3)$ 57. The assignment of the NMe resonance was confirmed by turning off the decoupler. ^{13}C NMR (75 MHz, 22 °C, toluene-d_8, at natural abundance ^{13}C, with $Cr(acac)_3$ as a shiftless relaxation agent): $\delta(W_4C)$ 366.8 (s, no satellites due to coupling to ^{183}W were discernible). Mass spectrum: a molecular ion envelope centered at m/e 1485 in the low-resolution electron

(26) (a) Fenske, R. F. *Prog. Inorg. Chem.* **1976**, *21*, 179. (b) Fenske, R. F. *Pure Appl. Chem.* **1971**, *27*, 61.

(27) Bursten, B. E.; Jensen, J. R.; Fenske, R. F. *J. Chem. Phys.* **1978**, *68*, 3320.

(28) Hehre, W. J.; Steward, R. F.; Pople, J. A. *J. Chem. Phys.* **1969**, *51*, 2657.

(29) Pickett, C. J. *J. Chem. Soc., Chem. Commun.* **1985** 323.

impact (EI) mode by selective ion monitoring (SIM). Cyclic voltammetry performed in 0.2 M Bu_4NBF_4 in THF at 22 °C revealed a reversible reduction at $E_+ = -1.7$ V vs. SCE and an irreversible oxidation at +0.17 V vs. SCE, $\Delta E_+ = 163$ mV; Fc/Fc^+ couple = +0.54 V, $\Delta E_+ = 151$ mV. Anal. Calcd for $W_4O_{12}NC_{38}H_{87}$: C, 30.72; H, 5.91; N, 0.94. Found: C, 30.55; H, 5.85; N, 0.87.

(2) $W_2(NMe_2)_6$ (500 mg, 0.79 mmol) was dissolved in a solvent mixture of hexane (5 mL) and CH_2Cl_2 (5 mL). *i*-PrOH (0.62 mL, 8 mmol) was added and the solution stirred at ambient temperature for ca. 12 h. The solvent was removed in vacuo, the solid dissolved in a 1:1 hexane/*i*-PrOH solvent mixture, and the solution cooled to 0 °C. Crystalline $W_4(O\text{-}i\text{-}Pr)_{12}$ was obtained and removed by filtration. ^1H NMR spectroscopy revealed the presence of $W_4C(NMe)(O\text{-}i\text{-}Pr)_{12}$ in the filtrate.

Procedure II. In a Schlenk reaction vessel 1.0 g of $W_2(NMe_2)_6$ was taken up in a slurry of hexane (30 mL) and excess *i*-PrOH (10 mL) added via cannula transfer. This was followed immediately by addition of py (2 mL) and stirred at room temperature. After 3 h, the reaction solvents were removed in vacuo to leave crude $W_2(O\text{-}i\text{-}Pr)_6(py)_2$ as a brown powder. The $W_2(O\text{-}i\text{-}Pr)_6(py)_2$ generated in this fashion from pure $W_2(NMe_2)_6$ is generally quite pure by ^1H NMR spectroscopy. When 0.55 g (0.62 mmol) of this $W_2(O\text{-}i\text{-}Pr)_6(py)_2$ was dissolved in hexane, concentrated, layered with DME, and cooled to −15 °C, a small crop of crystals of $W_4C(NMe)(O\text{-}i\text{-}Pr)_{12}$ was obtained after 12 h (0.05 g, 5% based on W).

Reaction of $W_2(\mu\text{-}^{13}CO)(O\text{-}t\text{-}Bu)_6$ with $W_2(O\text{-}t\text{-}Bu)_6$ and *i*-PrOH. Several approaches to this general reaction have been attempted, and the most fruitful of these are outlined as follows.

Procedure I. In a Schlenk reaction vessel $W_2(O\text{-}t\text{-}Bu)_6$ (0.50 g, 0.62 mmol) was taken up in hexane (ca. 35 mL) and cooled to 0 °C to give a deep red solution. To the stirred solution was added exactly 0.5 equiv (0.31 mmol) of ^{13}CO via a Hamilton gas-tight syringe. This was accompanied by an immediate precipitation of red, microcrystalline $W_2(\mu\text{-}^{13}CO)(O\text{-}t\text{-}Bu)_6$. The solution was stirred at 0 °C to ensure complete reaction of ^{13}CO to form 0.5 equiv of $W_2(\mu\text{-}^{13}CO)(O\text{-}t\text{-}Bu)_6$. After 1 h excess *i*-PrOH (ca. 10 mL) was added to the cooled, stirred solution via cannula transfer, and the solution appeared to darken with time. After being stirred at 0 °C for 1 h, the solution was warmed to room temperature and allowed to stir. After 12 h at room temperature, the volume of solution was reduced by half and cooled to −15 °C which produced many small crystals after 3 days. These crystals were isolated by cannula filtration and dried in vacuo. When these crystals were dissolved in toluene-d_8, it was very evident that two types of crystal were present, one went into solution as a violet compound, $[W_2(^{13}CO)(O\text{-}i\text{-}Pr)_6]_2$, and the other was light green. ^1H NMR spectroscopy at 360 MHz revealed the presence of the known compound $[W_2(^{13}CO)(O\text{-}i\text{-}Pr)_6]_2$ and many new ^1H resonances. $^{13}C\{^1H\}$ NMR spectroscopy at 75 MHz revealed the presence of the known compound $[W_2(^{13}CO)(O\text{-}i\text{-}Pr)_6]_2$, δ 306 ($^1J_{W\text{-}C}$ = 164.0, 189.0 Hz), and a new resonance at δ 348 with four well-resolved satellites due to $^{183}W\text{–}^{13}C$ coupling, $^1J_{W\text{-}C}$ = 177, 160, 37, and 24 Hz.

Procedure II. Crystalline $W_2(\mu\text{-}^{13}CO)(O\text{-}t\text{-}Bu)_6$ (1 equiv) was mixed with 1 equiv of crystalline $W_2(O\text{-}t\text{-}Bu)_6$ and dissolved in hexane. At room temperature, excess *i*-PrOH was added with stirring. This mixture was allowed to stir at room temperature for 12 h, followed by the analogous workup in procedure I.

Acknowledgment. We are grateful to the Department of Energy, Chemical Sciences Division, for financial support. We thank Dr. S. Harris of Exxon Research and Development and Professor E. R. Davidson and Dr. D. Feller of the Indiana University Quantum Chemistry Group for helpful discussions. D. L. Clark is the recipient of the 1985–1986 Indiana University General Electric Foundation Fellowship. The VAX 11/780 is an NSF supported departmental facility, CHE-83-09446 and CHE-89-05851.

Registry No. $W_4C(NMe)(O\text{-}i\text{-}Pr)_{12}$, 96453-17-7; $W_2(NMe_2)_6$, 54935-70-5; $W_2(\mu\text{-}^{13}CO)(O\text{-}t\text{-}Bu)_6$, 107494-93-9; $W_4(C)(O)(O\text{-}i\text{-}Pr)_{12}$, 107539-25-3; $W_4(\mu\text{-}CO)_2(O\text{-}i\text{-}Pr)_{12}$, 95674-38-7.

Supplementary Material Available: A table of anisotropic thermal parameters, complete listings of bond distances and bond angels, and VERSORT drawings of the $W_4(C)(NMe)(O\text{-}i\text{-}Pr)_{12}$ molecule giving the atom number scheme (10 pages); a listing of F_o and F_c values (37 pages). Ordering information is given on any current masthead page.